Received: 13 May 2024 | Revised: 29 September 2024 | Accepted: 4 October 2024

DOI: 10.1002/qj.4882

Quarterly Journal of the Royal Meteorological Society RMetS

RESEARCH ARTICLE

The first kind of predictability problem of El Niño predictions in a multivariate coupled data-driven model

Bo Qin[1*] | Zeyun Yang[2] | Mu Mu[1,3] | Yuntao Wei[1,4] | Yuehan Cui[5] | Xianghui Fang[1,6] | Guokun Dai[1,7] | Shijin Yuan[5]

[1]Department of Atmospheric and Oceanic Sciences & Institute of Atmospheric Sciences, Fudan University, Shanghai, China

[2]Key Laboratory of Ministry of Natural Resources for Marine Environmental Information Technology, National Marine Data and Information Service, Ministry of Natural Resources, Tianjin, China

[3]Shanghai Frontiers Science Center of Atmosphere-Ocean Interaction, Fudan University, Shanghai, China

[4]Shanghai Key Laboratory of Ocean-land-atmosphere Boundary Dynamics and Climate Change, Fudan University, Shanghai, China

[5]School of Computer Science and Technology, Tongji University, Shanghai, China

[6]CMA-FDU Joint Laboratory of Marine Meteorology, Shanghai, China

[7]Key Laboratory of Polar Atmosphere-ocean-ice System for Weather and Climate, Ministry of Education, Fudan University, Shanghai, China

Correspondence
Mu Mu, Department of Atmospheric and Oceanic Sciences & Institute of Atmospheric Sciences, Fudan University, Shanghai 200438, China.
Email: mumu@fudan.edu.cn

Funding information
National Natural Science Foundation of China, Grant/Award Numbers: 42288101, U2142211, 42405147, 42405048, 42475054; National Key Research and Development Program of China, Grant/Award Number: 2020YFA0608802; China National Postdoctoral Program for Innovative Talents, Grant/Award Number: BX20230071; TianHe Qingsuo Project special fund project in the field of clmate, meteorology, and ocean

Abstract

El Niño-Southern Oscillation (ENSO) is the dominant atmosphere–ocean coupled mode of year-to-year variations in the tropical Pacific. It shows diverse spatiotemporal characteristics and casts major influences on seasonal predictions of global weather–climate extrema. Despite numerous dynamical and statistical models for ENSO prediction and predictability studies, they are commonly subjected to one-to-three issues among less skillful simulation of El Niño diversity, huge requirements of computational resources and a low robustness in statistics. Here, an efficient deep-learning model involving nonlinear coupling of multiple variables is independently developed to study the predictability of two types of El Niño events related to initial uncertainty, which is the first kind of predictability problem. The model can skillfully simulate statistically robust features of observed El Niño diversity in terms of periodicity, amplitude, and seasonal phase-locking. Using this model, we have revealed mathematically several new types of fastest-growing initial errors in two types of El Niño predictions based on a novel concept of conditional nonlinear optimal perturbation (CNOP), especially including one that can strengthen central Pacific types of events, which is rarely investigated before. Moreover, CNOPs are superimposed into a numerical model, GFDL CM2p1, for comprehensive validation and growth mechanism mining, which demonstrates the consistent dynamical evolution of initial errors in both numerical and AI models. Our study represents the first attempt to explore the first kind of ENSO predictability problem from perspectives of nonlinear error-evolving dynamics using a data-driven model. This is of great importance as it offers us sufficient confidence to perform ENSO-related (such as the Madden–Julian Oscillation, etc.) mechanisms and predictability studies in the future without strongly relying on dynamical numerical models.

KEYWORDS

conditional nonlinear optimal perturbation, deep learning, ENSO diversity, ENSO prediction, ENSO's first kind of predictability problem

Bo Qin and Zeyun Yang contributed equally to this study.

1 | INTRODUCTION

As the dominant interannual variations in the tropical air–sea system, the El Niño-Southern Oscillation (ENSO) phenomenon (Philander, 1983) could largely impact global weather and climate. There is a consensus that El Niño can be classified into two types in terms of the location of maximum sea surface temperature (SST) anomalies, that is, the eastern Pacific (EP) type and the central Pacific (CP) type, and these two types of El Niño events have significantly different predictabilities. According to the two kinds of predictability problems proposed by Lorenz (1962), the forecast uncertainties of El Niño diversity mainly derive from the initial perturbation (i.e., the first kind of predictability problem) and the parameter perturbation (i.e., the second kind of predictability problem). Revealing optimal perturbations in either initial states or model parameters that affect predictions of El Niño diversity to the largest extent can further improve forecast skills via targeted observations and data assimilation.

For decades, many researchers have been devoted to investigating these two problems based on numerical models or statistical models, achieving significant progress. Based on linear approaches (e.g., linear singular vectors, LSVs), the states of the equatorial and off-tropical Pacific can significantly influence simulations of the two types of El Niño events (Pegion et al., 2020; Vimont et al., 2014). To fully consider the potential effects of nonlinearity intrinsic to the atmosphere–ocean, Mu et al. (2003) propose a novel concept of conditional nonlinear optimal perturbation (CNOP), which extends canonical LSVs into nonlinear fields. CNOPs represent the most potential precursor signals that lead to onsets of high-impact weather–climate events (Mu & Duan, 2003; Wei et al., 2019) or the fastest (i.e., optimally) growing initial errors (OGIEs) in affecting predictions (Dai et al., 2023; Tao et al., 2023; Wang et al., 2013). Benefiting from CNOPs, for example, the above-mentioned two kinds of predictability problems have been widely investigated in either intermediate coupled models or global coupled models, revealing the initial errors closely related to the Spring Prediction Barrier (SPB) in the two types of El Niño events via the CNOP method (Hu & Duan, 2016; Qi et al., 2021; Tao et al., 2022), and unraveling the effects of off-tropical air–sea coupling and three-dimensional ocean states on El Niño diversity (Hou et al., 2019; Yang et al., 2020, 2023).

However, most models applied in these studies often encounter the bottlenecks of weak simulation capability for El Niño diversity, especially for CP El Niño events (Lee et al., 2021). It has hindered comprehensive investigation into the predictability of this new type of El Niño. Even though there have been several effective and universal approaches that can compensate for the simulation capabilities of the numerical models, such as the nonlinear forcing singular vector (NSFV) method (Duan et al., 2014, 2018; Duan & Zhao, 2015; Tao et al., 2020; Tao & Duan, 2019), the sophisticated nonlinear optimization in these studies usually costs huge time and computing resources.

With the advent of the artificial intelligence (AI) era, some data-driven deep-learning ENSO forecasting models (Ham et al., 2019) are developed and put into operational routines, such as Geoformer (Zhou & Zhang, 2023), ENSO-GTC (global teleconnection coupler) (Mu et al., 2022b), and ENSO-ASC (air–sea coupler) (Mu et al., 2021). From a statistical perspective, such a data-driven ENSO forecasting model specifically learns hierarchical representations of multivariate data through neural networks with numerous layers (Bengio et al., 2013; Schmidhuber, 2015; Zhang et al., 2021), bridging a complex nonlinear mapping between historical and future states from simulations, reanalysis, and/or observations. According to substantial evaluations of hindcasts and forecasts, they can usually provide a skillful prediction for lead times longer than one and a half years, beyond most numerical models. These models can also distinguishably predict two types of El Niño events to some extent, which indicates they may implicitly learn reliable physical mechanisms from data. Simultaneously, their efficiency and consumption are undoubtedly reduced by being deployed on specialized devices. For example, simulating a year in these models usually takes only a few minutes, while taking one to three hours in global coupled models.

According to the characteristics of neural networks in deep-learning models, it can be inferred that such model's inputs and outputs are in one-to-one deterministic correspondence, which means uncertainties in the initial states can definitely induce uncertainties in the forecast results and affect the prediction of El Niño diversity. Therefore, forecast errors of two types of El Niño events in well-trained deep-learning models originate more from the initial error rather than the model parameters, which belongs to the first kind of predictability problem. Reducing such initial errors in the model's inputs can further improve the practical forecast skills.

In this study, we attempt to reveal OGIEs for the prediction of ENSO in a data-driven model via the CNOP method. The optimization of CNOPs in data-driven models can be supported by "automatic differentiation" (Ketkar et al., 2021). OGIEs usually cause the largest forecast error and exhibit specific spatial patterns, the reduction of which in the initial conditions by targeted observation and data assimilation holds valuable significance in practical operational forecasts for data-driven models. Additionally, the utilized data-driven model should possess interpretability to some extent, or at the

very least, it should have a superior simulation capability for El Niño diversity.

To this end, we choose ENSO-MC (multichannel) constructed by us before (Mu et al., 2022a) as the basis to reveal OGIEs of two types of El Niño events, which can evolve the monthly averaged spatial variations for sea surface temperature (SST), the average sea temperature in the upper 300 m (T300), and surface zonal/meridional wind (U/V-Wind) over the Pacific region (40°N–40°S, 120°E–80°W). We modify this model in terms of the training dataset, forecasting strategy, and model structures to raise its forecast skill (i.e., Niño3.4 index correlation skill) to 0.81/0.67/0.51 within 6/12/17 lead months compared to the previous 0.64/0.53/0.48, accompanied by discriminative simulation capability for two types of El Niño events. The upgraded model is marked as ENSO-MC v2.0. Subsequently, we solve CNOPs in ENSO-MC v2.0 to reveal several new types of OGIEs for two types of El Niño events as shown in Figure 1a, and superimpose the obtained OGIEs into a numerical model, GFDL CM2p1 (Delworth et al., 2006), to interpret their growth mechanisms as shown in Figure 1b. GFDL CM2p1 has discriminative simulation capability for two types of El Niño events (Ham & Kug, 2012; Kug et al., 2010). The experimental results demonstrate these CNOP-based initial errors keep consistent nonlinearly evolving dynamics as those obtained from numerical models, especially the one that can strengthen CP events, which has been never investigated before.

Our study confirms that CNOP method can be applied in skillful data-driven ENSO forecasting models to perform the first kind of predictability study, the results of which can be effectively verified in numerical models. Meanwhile, this application can be migrated to other weather/climate phenomena (e.g., Madden–Julian Oscillation, Quasi-Biennial Oscillation, etc.) for a series of challenging predictability problems, with the help of high efficiency and performance of deep learning.

The rest of this paper is organized as follows. Section 2 describes ENSO-MC v2.0 and the method of how to solve CNOPs in it. Section 3 demonstrates comprehensive evaluations of our upgraded ENSO-MC v2.0. Section 4 outlines several new types of OGIEs obtained from ENSO-MC v2.0 with their dynamical interpretability. A discussion and summary are provided in Section 5.

2 | DATA, MODEL AND METHOD

2.1 | Data

The training data for ENSO-MC v2.0 are extended from the reanalysis to simulation data for the period 1850–2014 as shown in Figure 2a, and complement a more comprehensive coverage of seasonal and interannual

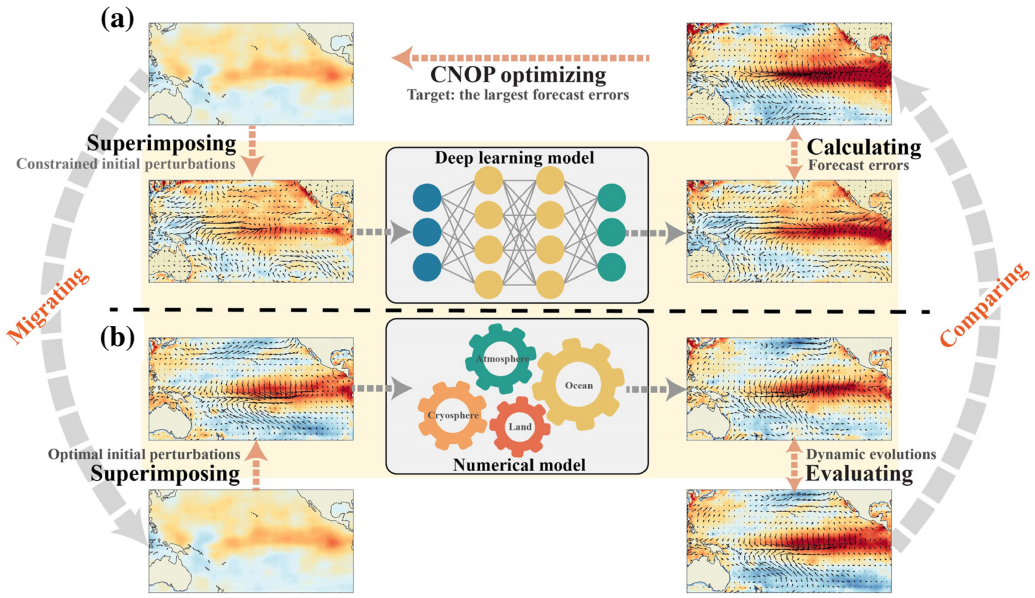

FIGURE 1 The procedures for (a) revealing the optimally growing initial errors (OGIEs) in a deep-learning El Niño-Southern Oscillation (ENSO) forecasting model and (b) evaluating the results in numerical models. The skillful deep-learning climate/weather models usually have higher forecasting/simulating skills with much lower computational resource and time consumption, which can be regarded as an effective tool for predictability studies of various complex phenomena via the conditional nonlinear optimal perturbation (CNOP) method. The proposed process contains two essential procedures, one for optimizing CNOPs in deep-learning models, and another for verifying the correctness of the obtained results in dynamical numerical models, highly maintaining reliability. [Colour figure can be viewed at wileyonlinelibrary.com]

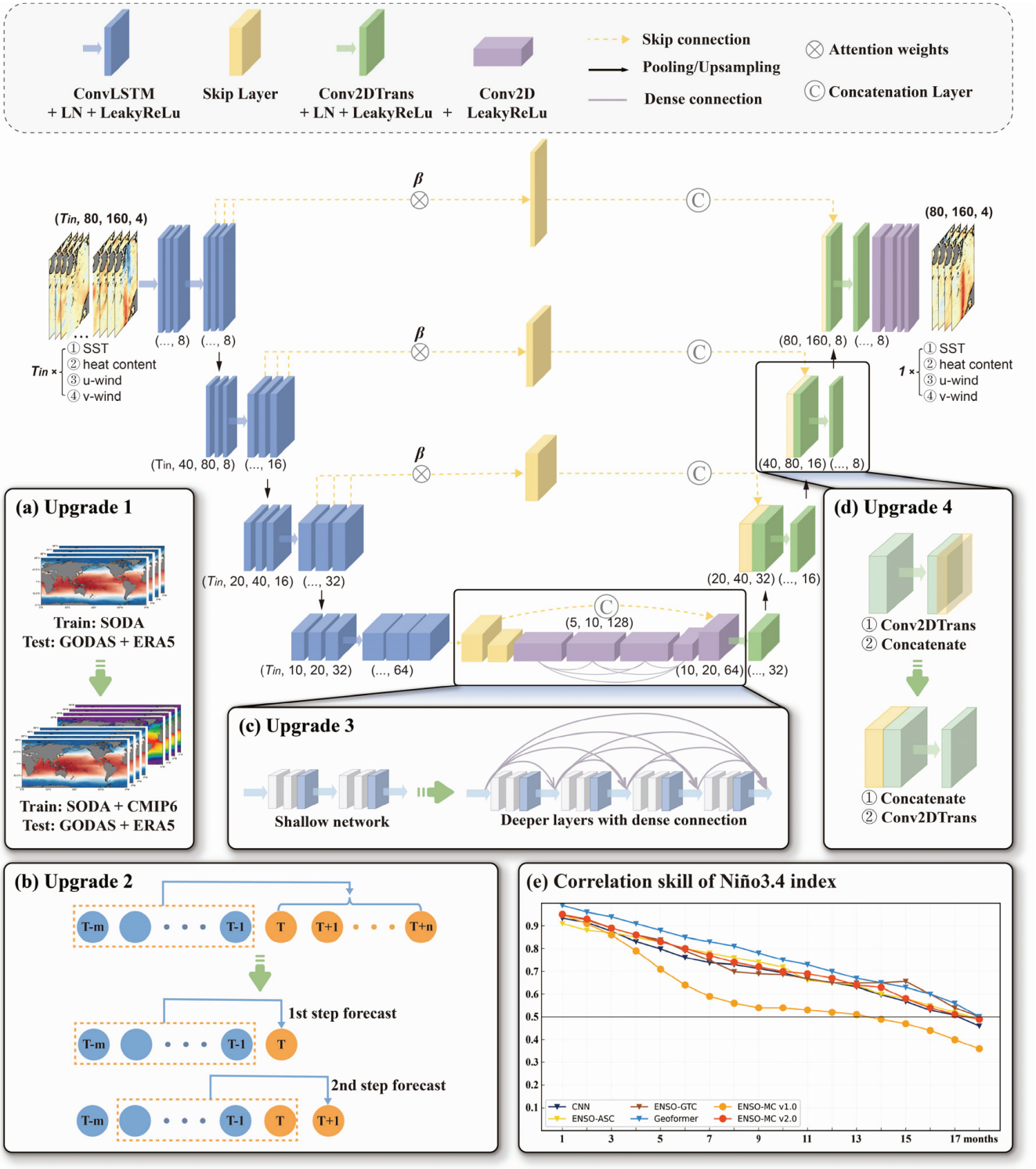

FIGURE 2 The detailed architecture and four major upgrades of El Niño-Southern Oscillation-multichannel (ENSO-MC) v2.0. Two macro upgrades are the (a) training datasets and (b) iterated forecasting strategy. Two micro upgrades contain (c) dense connection middle layers and (d) a switch of skip-layer connection and transpose convolution layer. (e) The Niño3.4 correlation skill of ENSO-MC v2.0 (orange line) compared to others, which is over 0.67/0.51 within the 12−/17-month leading time. [Colour figure can be viewed at wileyonlinelibrary.com]

changes, accompanied by more infrequent and extreme events, raising the generalization and inference capabilities of ENSO-MC v2.0. As shown in Table 1, all selected CMIP6 and SODA data are used as the training set, while GODAS (SST and T300) and ERA5 (surface wind) data from 1980 to 2022 serve as the testing set. The

TABLE 1 Details of the CMIP6 simulations and reanalysis data used for training and testing of El Niño-Southern Oscillation-multichannel (ENSO-MC) v2.0.

No	CMIP6 model source	Modeling group	Period
1	ACCESS-CM2	CSIRO-ARCCSS	January 1850–December 2014
2	CAMS-CSM1-0	CAMS	
3	CESM2	NCAR	
4	CESM2-WACCM	NCAR	
5	E3SM-1-1	E3SM-Project RUBISCO	
6	FGOALS-g3	CAS	
7	FIO-ESM-2-0	FIO-QLNM	
8	GFDL-CM4	NOAA-GFDL	
9	NESM3	NUIST	
10	NorESM2-MM	NCC	

No	Reanalysis data	Institution	Period
1	SODA	University of Maryland	January 1871–December 1979
2	GODAS	NCEP	January 1980–December 2022
3	ERA5	ECMWF	January 1980–December 2022

Note: We first used numerous multisource multivariate data to train the model and tested the model performance on GODAS and ERA5. The yellow colored background represents the simulation data, and the red colored background represents the reanalysis data.

spatial domain covers 40°N–40°S, 120°E–80°W. All data are preprocessed into monthly averages and interpolated into a regular grid with a resolution of $1° \times 1°$, and all land grids and missing values are assigned a value of 0.

2.2 | The deep-learning model

The detailed architecture of ENSO-MC v2.0 is shown in Figure 2, which resembles its original version. The neural network modules and tensor shape variations are marked in this plot. All contained variables are stacked along the channel, and the input length is set as 12 months. We choose ENSO-MC as the basis because of its adequate variables (i.e., SST, T300, U/V-Wind) and reasonable coverage region (i.e., 40° N–40° S, 120° E–80° W) compared with Geoformer (covering 20° N–20° S), ENSO-ASC (not possessing vertical ocean information), and ENSO-GTC (only possessing SST), which facilitates comprehensively characterizing the air–sea coupled interactions among multilayers of sea surface, subsurface, and near-surface.

The forecasting strategy is shifted to the iterative strategy by outputting the multivariate result for the next month, which is then fed into the model's input for the subsequent month's predictions (Figure 2b). Compared to the direct strategy used in the original version, the iterative strategy aligns more closely with the physical laws in meteorology, fully utilizing inferential and memorized information from all previous sequences via the skeleton of convolutional long- and short-term memory (ConvLSTM) (Shi et al., 2015) and offering more flexibility in predicting an arbitrary number of steps.

To further enhance the resolving and presentation capability in simulating the nonlinear system of ENSO, ENSO-MC v2.0 has deepened the first and last layers of the whole network. Dense connections (Huang et al., 2017) are employed between encoder and decoder (Figure 2c) with several convolution layers (shown by purple networks), allowing direct interconnectivity between each layer and all preceding layers for more effective learning and extraction of complex features. Additionally, ENSO-MC v2.0 departs from the original model's approach of performing deconvolution before concatenating with the feature map of the skip connection layer. In the upgrade version, each layer of the decoder first concatenates with the corresponding skip layer, followed by deconvolution (Figure 2d). This change in the connection order allows for the integration of contextual information from the skipped connections at a lower resolution. As a result, by the time deconvolution occurs, the network has already assimilated a rich combination of contextual and local features, thereby enhancing the model's ability to integrate contextual information more effectively.

2.3 | CNOP method

Conditional nonlinear optimal perturbation refers to the optimal initial perturbation under a certain constraint that can cause maximum forecast error at the forecasting time. It can be formalized as a nonlinear optimization problem $J(\cdot)$ mathematically as Equation (1), where $u_\delta'^*$ is obtained CNOP, ϵ is the constraint radius, M_τ represents the nonlinear system (e.g., ENSO-MC v2.0 in our study) with integral τ steps, u_0 and u_δ' represent its initial condition and initial perturbation. u_δ' is also the variable to be optimized. The ℓ-norm is used to measure the forecast errors.

$$\begin{cases} J\left(u_\delta'^*\right) = \max\limits_{\|u_\delta'\|_\ell \le \epsilon} \left\|u_\tau'\right\|_\ell \\ u_\tau' = M_\tau\left(u_0 + u_\delta'\right) - M_\tau(u_0) \end{cases} \tag{1}$$

Solving CNOPs for deep-learning models is relatively more convenient compared with dynamical numerical models. With the help of "automatic differentiation

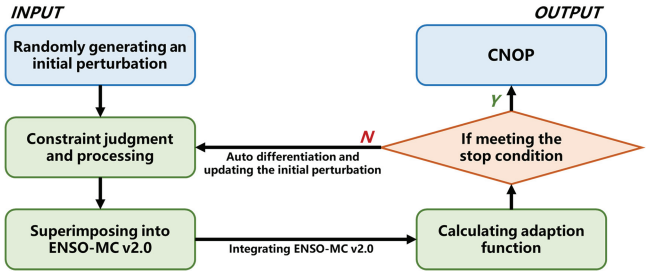

FIGURE 3 The flowchart for solving conditional nonlinear optimal perturbations (CNOPs) for El Niño-Southern Oscillation-multichannel (ENSO-MC) v2.0. The parameters of ENSO-MC v2.0 are unchanged during this optimization. [Colour figure can be viewed at wileyonlinelibrary.com]

(Ketkar et al., 2021)" of almost all deep-learning programming frameworks (e.g., Tensorflow [Shukla & Fricklas, 2018], PyTorch [Stevens et al., 2020], etc.), the gradient of $J(\cdot)$ can be calculated easily. The flowchart for solving CNOP in ENSO-MC v2.0 is shown in Figure 3 after obtaining the well-trained model. A randomly generated trainable parameter (i.e., initial perturbation) is superimposed on the initial condition of ENSO-MC v2.0. Then, the adaption function $J(\cdot)$ is calculated after integrating the model with the perturbed initial condition. Finally, the initial parameter is gradually optimized until satisfying the stop condition, guided by the gradient of $J(\cdot)$ via "automatic differentiation." More importantly, the parameters of ENSO-MC v2.0 should be "frozen" (i.e., they are set to be untrainable) during the optimization of CNOP.

During implementation, we add the initial perturbation u'_δ on the January initial SST of the selected reference cases, and calculate the adaption function $J(\cdot)$ on SST in December after iterating ENSO-MC v2.0 for 11 times. This fits with the common seasonal phase-locking that ENSO onsets in January and reaches peaks in December. The paradigm ℓ for adaption function $J(\cdot)$ is set to 2. The constraint radius is set to 10% of the 2-paradigm of GODAS SST climatology (1980–2010). This ensures solid evolutions and consistent physical significances of the initial errors, preventing the pattern collapse of the deep-learning model. In addition, to capture the initial perturbations that produce the greatest impacts on the prediction of El Niño diversity, we define the calculated regions of $J(\cdot)$ as Niño3 and Niño4 regions, respectively for EP and CP events, considering the distinct positions of the most active SST anomalies (SSTA) in their mature phases.

All widely confirmed EP (i.e., 1982, 1986, 1991, 1997, 2006, and 2014) and CP (i.e., 1994, 2002, 2004, 2009) events are selected as reference states, all of which are well simulated by ENSO-MC v2.0. Because our designed adaption function for CNOP optimization is an equation for the 2-paradigm (i.e., $\ell = 2$), which focuses on the magnitudes, not the directions of prediction errors induced by initial perturbations, the obtained CNOPs tend to be divided into two categories mathematically, or rather, one each for strengthening and weakening the intensity of the reference state. We conduct optimizations 100 times for every reference state, then sort them into descending order to select the top-50 results for constituting the CNOP candidate set (the top-50 represents relatively well-optimized and reliable results), then average them with the same properties (strengthening and weakening) to obtain spatial patterns for OGIEs.

2.4 | Heat budget analysis

We evaluate the effects of the cobtained OGIEs in GFDL CM2p1 and perform the heat budget analysis on simulation results to better interpret the growth mechanisms of initial perturbations distributed in the equatorial Pacific. Especially, we focus on three key terms: total temperature tendency, thermocline feedback, and zonal advection feedback as defined in Equations (2)–(4), where T and u represent the averaged sea temperature and zonal current velocity in the ocean'S upper 55 m, w represents the vertical current velocity at the depth of 55 m, dt, ∂x, and ∂z are time intervals (one month), zonal grid width (25 km) and vertical grid width (10 m) in GFDL CM2p1, $\bar{\cdot}$ and $\cdot'$ represent the climatology and error, respectively. The latter two terms with related dynamical processes could contribute differently to two types of El Niño events, benefiting the mining of distinguishable features of different types of OGIEs.

$$\text{Total temperature tendency: } {}^{dT}/_{dt} \tag{2}$$

$$\text{Thermocline feedback: } -\overline{w}\,{}^{\partial T'}/_{\partial z} \tag{3}$$

$$\text{Zonal advection feedback: } -u'\,{}^{\partial \overline{T}}/_{\partial x} \tag{4}$$

In addition, we also define two indicators, wind speed error index and latent heat flux error index (i.e., the average wind speed error and latent heat flux error over the region 10° N – 20° N, 150° W – 120° W), to better understand the propagation mechanism of the significant initial perturbations in the off-equatorial northern Pacific.

3 | PERFORMANCE EVALUATIONS OF ENSO-MC V2.0

3.1 | Evaluations on simulation capability

High simulation skills facilitate CNOP-basedpredictability studies, which favor tracking dynamical evolutions

for initial perturbations. We evaluate the physical characteristics of produced ENSO events by our model during long-term simulations. We choose every month's data from 2000 to 2009 as the initial conditions to generate a total 12,000-year simulation (100-year simulation for each initial condition). More precisely, for each 100-year simulation, the portion that coincides with the observational period can also be called hindcasts, and the remainder can be regarded as forecasts. Since the iterative steps for 100 years far exceed the model's effective lead months (see Section 3.2), we refer to these hindcasts with forecasts as simulations, and compare them with observations statistically.

First of all, we extract all EP and CP events respectively in this long simulation, and average them. The individual Hovmöller diagrams (5° S – 5° N latitudinal average) are shown in Figure 4. The seasonal phase-locking is obvious, and the maximum centers of SSTA are discriminative for two types of events, which lie near 120° W for EP events, and near the dateline for CP events. The intensity (i.e., SSTA amplitude) of the EP event is stronger than that of the CP event in general. In more detail, we intercept three 20-year intervals to show the irregular oscillations, as in Figure A1. The extremely strong El Niño events always belong to the EP type and appear about every 10 years, and La Niña events tend to be continuous like in recent years. Such results illustrate the superior grasp of complex ENSO similar to the real world (Iwakiri & Watanabe, 2021; Lopez et al., 2022).

Next, we quantify some statistical indicators concerning concrete physical meaning as shown in Figure 5. Note that the blue shadings (intervals of one standard deviation) and lines (averages) are composed of 120 segments, each of which spans 100 years. Overall, the statistical properties of ENSO-MC v2.0 (blue lines) are very similar to the observations (green lines). Specifically, Figure 5a,d shows the power spectrums of Niño3 and 4 indexes, respectively. Both of them exhibit a subpeak around 1.5 years and a peak between four and six years. The former matches the sub-ENSO variabilities (Keenlyside et al., 2007), and the latter is consistent with the major interannual oscillations. In addition, the peak value for the power spectrum of the Niño3 index is larger than that of the Niño4 index, implying a stronger amplitude for EP events. Figure 5b,e shows probability distributions of Niño3 and Niño4 indexes, respectively. Both of them display Gaussian-like but asymmetric shapes. The distribution of the Niño3 index contains a long tail in the positive intervals compared with that of the Niño4 index, suggesting the more likely occurrences of extreme EP events than CP events. The skill for cold events is relatively weak in our model, with a slight intensity underestimation as shown in the negative axis of both distributions. Figure 5c,f shows the monthly variances of Niño3 and 4 indexes, respectively. The variations

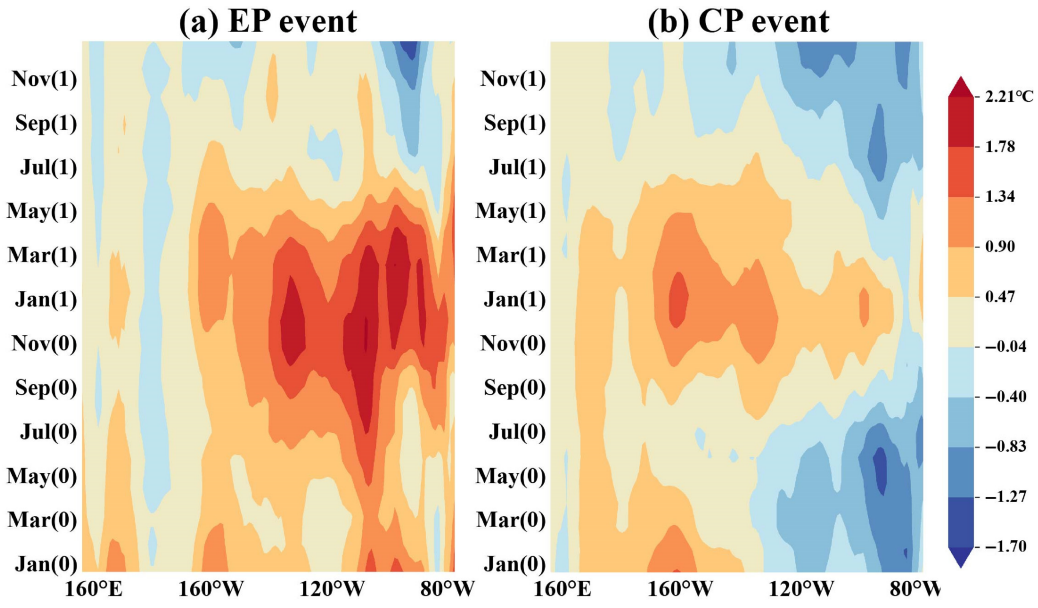

FIGURE 4 Hovmöller diagrams for the composited (a) eastern Pacific (EP) event and (b) central Pacific (CP) event in the long-term simulation of El Niño-Southern Oscillation-multichannel (ENSO-MC) v2.0. They are both the average of the 80 extracted corresponding events in a 1000-year simulation, respectively. The mature phases of these two types of events are both in the boreal winter (December–January–February), and the sea surface temperature anomaly (SSTA) centers of them are discriminative. The SSTA amplitude of the EP event is stronger than that of the CP event in general. [Colour figure can be viewed at wileyonlinelibrary.com]

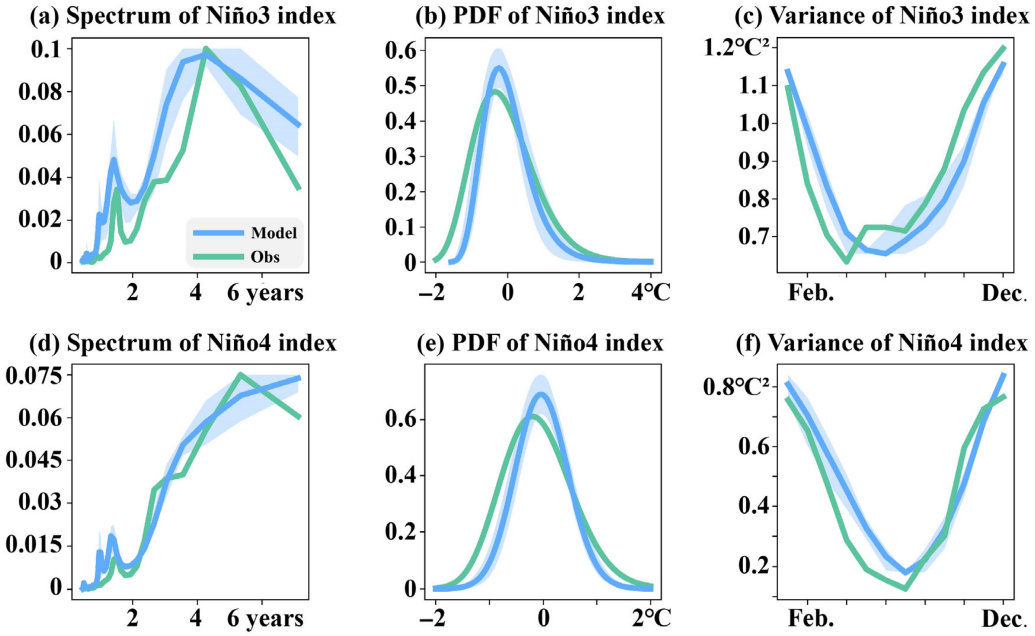

FIGURE 5 Comparisons between the physical statistics of the long-term simulation of El Niño-Southern Oscillation-multichannel (ENSO-MC) v2.0 (blue lines and shading) and observations (green lines). (a,b) Power spectrums of Niño3 and Niño4 indexes. (c,d) probability density functions of Niño3 and Niño4 indexes. (e,f) Monthly variance of Niño3 and Niño4 indexes. The blue shadings represent the one-standard-deviation intervals and the blue lines represent averages. The periods, intensities, and seasonal synchronizations for different types of events simulated by ENSO-MC v2.0 are almost the same as observations. [Colour figure can be viewed at wileyonlinelibrary.com]

tend to be the same with the onset in spring, development in summer/autumn, and maturity in winter, capturing the seasonal phase-locking features. ENSO-MC v2.0 also reproduces the slightly later (there is around a one-month delay between their valleys) onset for CP events than EP events, which shrinks the growing period and corroborates to explain the absence of extreme CP events (Yu et al., 2017). However, this difference is not as significant as the observations.

According to the above assessment, we have confirmed that the simulations of ENSO-MC v2.0 are consistent with naturally occurring ENSO events to a large extent, learning the concrete dynamical mechanisms of two types of El Niño events. Such evaluations provide high confidence for the subsequent two types of El Niño predictability study based on ENSO-MC v2.0, a deep-learning model.

3.2 | Evaluations on hindcast skill

Figure 2e demonstrates the Niño3.4 index correlation skills varying with forecasting lead months. ENSO-MC v2.0 can provide effective hindcasts (i.e., correlation skill is greater than 0.65) up to 12 lead months, surpassing the original version (around six months) to a large extent. If adopting 0.5 as the threshold value for effective hindcasts, the skill for ENSO-MC v2.0 also lasts up to 17 months, side-by-side with other current ENSO deep-learning models of first-tier level (Mu et al., 2021, 2022b; Zhou & Zhang, 2023).

The long-term hindcasts from 2000 to 2022 with different lead months and a forecast starting from September 2023 are shown in Figure 6a,b. ENSO-MC v2.0 has a better capture of the intensity of the extremely strong El Niño events (i.e., 15/16) despite a leading time under 12 months. In addition, it has to be mentioned that ENSO-MC v2.0 tends to underestimate the intensity of La Niña events. It seems that the hindcast skill for the second consecutive La Niña event is slightly higher than the first transition into the cold state, which is also reflected in other deep-learning models, such as Geoformer exhibiting better skills when starting forecasting in late 2020 and 2021 (Gao et al., 2023). In other words, when the input sequence is already in the cold phase, deep-learning models preserve the cold "memory" well; but when the input sequence is still in the warm phase, deep-learning models may avoid forecasting a rapid phase transition. Some studies indicate the important effect of subsurface temperature anomalies in sustaining prolonged La Niña events (Gao et al., 2022), suggesting that information augmentation and extraction from the subsurface layer should be enhanced in deep-learning models.

We also investigate its skill variations with different forecasting start calendar months, as shown in Figure 6c.

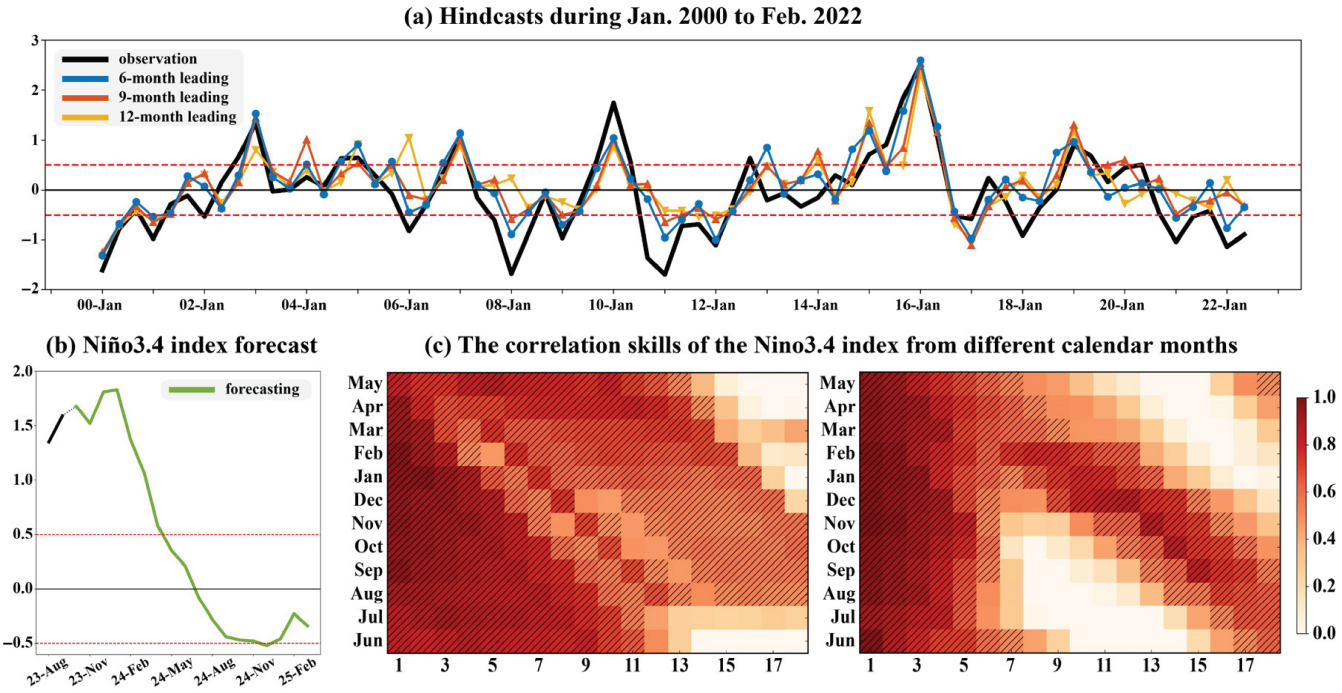

FIGURE 6 (a) Hindcasts (color lines) from 2000 to 2022 with different leading months compared to the observations (black line), and (b) a forecast from September 2023. (c) The correlation skills of the Nino3.4 index from different calendar months using El Niño-Southern Oscillation-multichannel (ENSO-MC) v2.0 on the left and ENSO-MC on the right, validated over the testing period. The hatched cells indicate predictions with correlation skill exceeding 0.5. [Colour figure can be viewed at wileyonlinelibrary.com]

Compared to the original model (right), the ENSO-MC v2.0 (left) demonstrates higher correlation skills for the Nino3.4 index across almost all target seasons. This improvement is particularly noticeable for target seasons approaching May and June. The skill decline is significant in the original model, highlighted by the light-shaded and band-like areas in the figure, which is attributed to the SPB. Yet such decline has been suppressed in ENSO-MC v2.0, which indicates ENSO-MC v2.0 can mitigate the effects of SPB to a large extent.

For more details, Figures A2 and A3 compare the spatial–temporal results with observations for four hindcast cases of two types of events respectively with 12 lead months. Our model can produce the grid results with high similarity to truth and can distinguish the differences in the location of maximum SSTA for different types of events well, and exhibits a consistent seasonal phase-locking with a tendency to peak during boreal winter.

In summary, ENSO-MC v2.0 can provide accurate and reliable simulating results for two types of El Niño events under 12 lead months, surpassing its original version. We believe there are two main reasons. Firstly, we use additional simulation data from multiple numerical models to train the model as some successful examples (Zhou & Zhang, 2023), which provides massive and diverse samples including extremes, making the AI model possess higher generalization. Secondly, we modify the neural network architecture of ENSO-MC to be more rational, empirically referencing previous work (Liu et al., 2022), increasing network capacity and performance. It is worth noting that the input sequence length of ENSO-MC v2.0 is still 12 months as its original version, which is reasonable. Shorter input sequence lengths lead to insufficient information, while longer input sequence lengths have significant marginal benefits and introduce noise (Zhang et al., 2024).

4 | OGIES FOR TWO TYPES OF EL NIÑO EVENTS

4.1 | The obtained OGIEs

The obtained OGIEs for two types of El Niño events are shown in Figures 7–9. Here, including the subsequent Figure 11, we display the "error" evolutions for the OGIE, which represent the differences between the reference states and the superimposed results. A distinction needs to be made with the common term "anomalies," which means the difference between reference states and climatology.

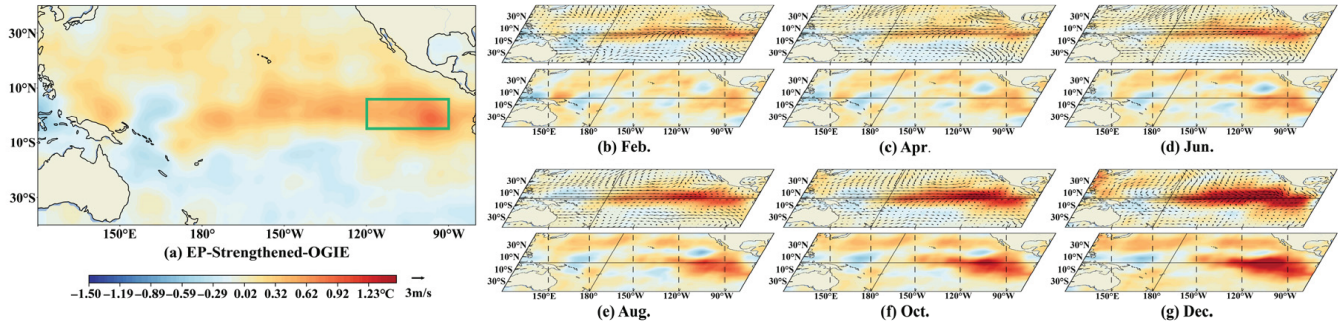

FIGURE 7 Eastern Pacific-Strengthened-optimally growing initial error (EP-Strengthened-OGIE) that can strengthen the EP events. (a) The spatial pattern of OGIE, which exhibits a significant positive sea surface temperature (SST) perturbation over the eastern equatorial Pacific in the green box. The upper/lower layers in (b–g) represent error evolutions of the sea surface/subsurface over February, April, June, August, October, and December, where the shadings represent SST/T300 errors and the vectors represent wind errors. [Colour figure can be viewed at wileyonlinelibrary.com]

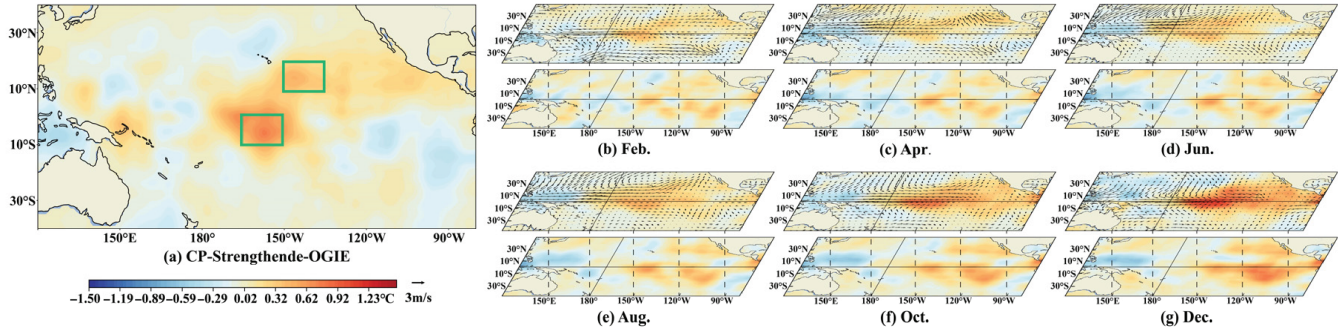

FIGURE 8 Central Pacific-Strengthened-optimally growing initial error (CP-Strengthened-OGIE) that can strengthen the CP events. (a) The spatial pattern of OGIE, which exhibits two significant positive sea surface temperature (SST) perturbations in the green boxes, one over the off-equatorial northern Pacific, and another over the central equatorial Pacific. The upper/lower layers in (b–g) represent error evolutions of the sea surface/subsurface over February, April, June, August, October, and December, where the shadings represent SST/T300 errors and the vectors represent wind errors. [Colour figure can be viewed at wileyonlinelibrary.com]

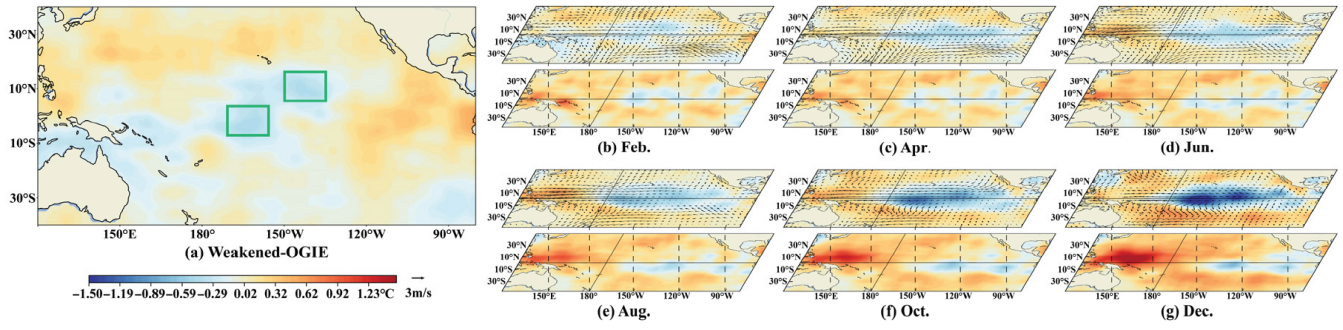

FIGURE 9 Weakened-optimally growing initial error (Weakened-OGIE) that can weaken two types of events. (a) The spatial pattern of OGIE, which is almost opposite to the central Pacific (CP)-Strengthened-OGIE of Figure 7. Two significant negative sea surface temperature (SST) perturbations are in the green boxes. The upper/lower layers in (b–g) represent error evolutions of the sea surface/subsurface over February, April, June, August, October, and December, where the shadings represent SST/T300 errors and the vectors represent wind errors. [Colour figure can be viewed at wileyonlinelibrary.com]

Figure 7a exhibits the OGIE that can strengthen EP events (marked as EP-Strengthened-OGIE), with the corresponding OGIE on the first panel and its evolutions following. The most crucial area for error distribution in this type of OGIE lies in the eastern equatorial Pacific (5° S – 5° N, 120° W – 90° W, shown as the green box)

under the 3-sigma rule (i.e., the cluster of grids, on which values deviate more than three times the standard deviation from the mean value). The extensive positive SST error concentrated in this area can directly weaken the west–east SSTA gradient of the reference states, which triggers the westerly wind errors as marked in Figure 7b–g, enhancing the Bjerknes feedback mechanism (Bjerknes, 1969). As a result, such OGIE further amplifies the positive SST errors over the equatorial Pacific, causing the enhancement of EP events. EP-Strengthened-OGIE has a similar significant maximum value region (in the green box) compared with the OGIE obtained in the improved Zebiak–Cane model by the NFSV method (Duan et al., 2018), which are both located in the eastern equatorial Pacific.

Figure 8a shows the OGIE that can strengthen the CP events (marked as CP-Strengthened-OGIE). The significant area for error distribution in this type of OGIE mainly lies in two parts under the 3-sigma rule, one of which is the central equatorial Pacific (7° S – 3° N, 165° W – 150° W of the lower green box), and the other is the off-equatorial northern Pacific (10° N – 20° N, 150° W – 135° W of the upper green box). Both of them exhibit strong positive errors. The northern positive SST errors can excite the local surface wind errors from February as shown in Figure 8b, and are propagating toward the central equatorial Pacific (Figure 8c–g). In addition, the westerly wind anomalies caused by the positive SST errors over the central equatorial Pacific also promote further amplification of these positive perturbations, causing the enhancement of CP events. This is a newly revealed type of OGIE, which has never appeared in numerical models.

The OGIEs that weaken EP and CP events are similar, so we combine them as averages as shown in Figure 9a (marked as Weakened-OGIE), and the distribution of the most significant areas is almost opposite to that of CP-Strengthened-OGIE. The slight difference lies in these two significant areas bwing more concentrated and closer to the central equatorial Pacific. One is located at 5° S – 5° N, 170° W – 155° W (the lower green box), and another is located at 5° N – 15° N, 150° W – 135° W (the upper green box). From the perspective of evolutions, the northern negative errors can excite the northeasterly wind anomalies from April (Figure 9c), with continuous southern propagation of local negative SST errors as shown in Figure 9c–g. Meanwhile, the development of the negative SST errors over the central equatorial Pacific is also significant from February (Figure 9b). Such variations lead to a La Niña-like evolution, causing serious weakening of reference states. The evolutions of initial errors in these two crucial areas (green box) in Weakened-OGIE

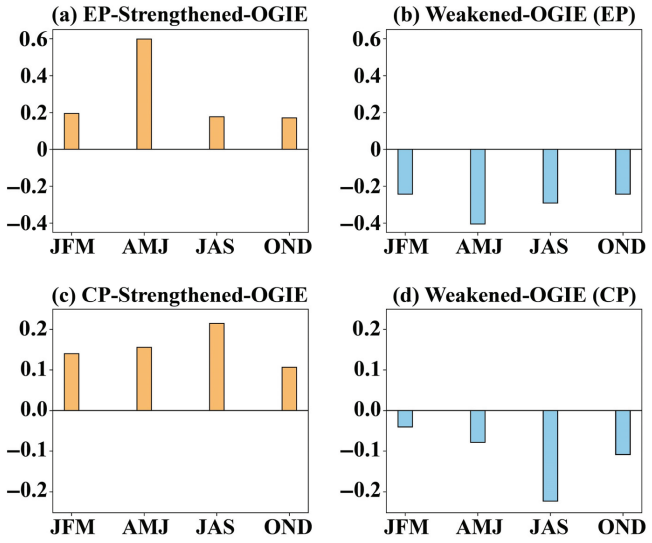

FIGURE 10 The seasonally-averaged growth rate of adaption values after superimposing the obtained three types of growth initial errors (OGIEs) into corresponding reference states (i.e., the chosen simulated eastern Pacific [EP] and central Pacific [CP] events) in El Niño-Southern Oscillation-multichannel (ENSO-MC) v2.0. (a, b) EP events, and (c, d) CP events. The color of bars indicates a positive (orange) or negative (blue) growth. [Colour figure can be viewed at wileyonlinelibrary.com]

exhibit similar dynamical mechanisms with significant perturbation developments in equatorial and northern Pacific of EP-Type-2 and CP-Type-2 kind of OGIEs revealed in CCSM4 (Hou et al., 2019).

ENSO prediction suffers from the predictability barrier phenomenon, which is strongly related to the characteristics of the initial error growth (Mu et al., 2007b). We also investigate the seasonally-averaged growth rate of adaption values after superimposing our obtained three types of OGIEs into corresponding reference states (i.e., the chosen simulated EP and CP events) in ENSO-MC v2.0, the results of which are shown in Figure 10. For EP events, the maximum growth rate occurs in April–May–June (AMJ) for both EP-Strengthened-OGIE (Figure 10a) and Weakened-OGIE (Figure 10b), consistent with the SPB in previous studies (Duan et al., 2009; Duan & Hu, 2016; Duan & Wei, 2013; Mu et al., 2007a; Xu et al., 2021). For CP events, the maximum growth rate exhibits in July–August–September (JAS) for both CP-Strengthened-OGIE (Figure 10c) and Weakened-OGIE (Figure 10d), consistent with a summer predictability barrier in some recent works (e.g., Ren et al., 2016). In addition, EP events have stronger error growth and more significant seasonal dependence than CP events as suggested by Ren et al. (2016). All the similarities above further validate the OGIEs obtained in this study.

4.2 | Verification using the GFDL CM2p1

Verifying the obtained OGIEs and the underlying physical mechanisms is quite crucial in the context of AI. The intuitive insight is to compare our patterns with previously identified OGIEs via CNOP in other numerical models. Existing studies are mostly concentrated on revealing OGIEs that weaken the intensity of two types of El Niño events, while OGIEs that strengthen the events are less investigated and limited to EP events only. For example, OGIEs for strengthening and weakening EP events in CESM in recent work (Xu et al., 2021) resemble our obtained EP-Strengthened-OGIE and Weakened-OGIE, but they have only identified the weakening type OGIE for CP events in this numerical model, which is also similar to the one that weakens the EP events. These OGIEs are consistent with the results revealed in our AI model. Exploration for identifying OGIEs that can strengthen CP events due to the weak simulation capability of numerical models is rare. However, our constructed ENSO-MC v2.0 can learn discriminative features of the two types of El Niño events from big data, which cannot be simulated numerically well so far. Therefore, we obtain the OGIE that can strengthen CP events for the first time, which could significantly influence predictions of ENSO diversity.

To thoroughly validate the obtained OGIEs, we perform a sensitive study using GFDL CM2p1. This numerical model has been proven to possess an outstanding ability to simulate two types of events, which is a global coupled numerical model (Yang et al., 2020, 2023). We first use bilinear interpolation to adjust the resolution of OGIEs corresponding to the latitude–longitude coordinates of GFDL CM2p1, then superimpose the preprocessed OGIEs onto the individual reference states in GFDL CM2p1, that is, EP and CP event year, tracking and comparing spatial–temporal error evolutions. To strictly adhere to the conditions for CNOP solving, which represents the sustained and monthly averaged SST perturbation in January, we add the OGIE-type initial error three times into the SST in January over the same region, while integrating GFDL CM2p1 to one year. This process is shown in Figure 11.

Figure 12 exhibits the three-month-averaged error evolutions of corresponding OGIEs (Figure 12a,b for EP events, and Figure 12c,d for CP events). The last column displays the related Niño3/4/3.4 index variations. The corresponding variations of three key terms in heat budget analysis and two customized indices are shown in Figure 13. Overall, all OGIEs can move the amplitudes of corresponding events in the intended directions in GFDL CM2p1 as in ENSO-MC v2.0.

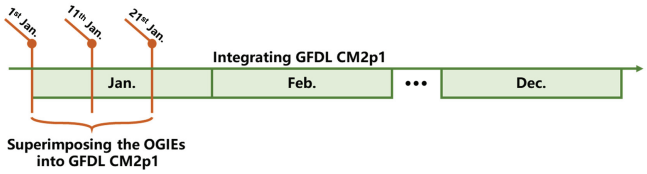

FIGURE 11 Schematic diagram for superimposing the obtained optimally growing initial errors (OGIEs) into the GFDL CM2p1 model. GFDL CM2p1 is integrated from 1 January and the obtained OGIEs are superimposed into this model three times in January, representing the sustained and monthly-averaged sea surface temperature (SST) perturbations. [Colour figure can be viewed at wileyonlinelibrary.com]

For EP-Strengthened-OGIE (Figure 12a), the significant initial positive perturbation concentrated over the eastern equatorial Pacific directly deepens the thermocline during January–February–March (JFM), accompanied by westerly wind anomalies across the equator and down-welling Kelvin waves. Such variations enhance the thermocline feedback in the Niño3 region from February and exert significant effects from June to September (Niño3 panel in Figure 13a), further improving the Bjerknes feedback in the reference state and amplifying the SST warming over the eastern equatorial Pacific in the mature phase. The contributions of zonal advection feedback are dominant in the Niño4 region (Niño4 panel in Figure 13a), which plays a major role from June to August and is consistent with westerly expansion of warm errors from the eastern equatorial Pacific. The effects of thermocline feedback in the Niño4 region can be ignored.

As for Weakened-OGIE in the EP event (Figure 12b), the negative SST error in the central equatorial Pacific, which induces easterly wind perturbations across the equator and upwelling Kelvin waves, plays a major role. Such variations weaken the thermocline feedback in the Niño3 region, especially after July–August–September (JAS) (Niño3 panel in Figure 13b). This perturbation weakens the original Bjerknes feedback in the reference state, slowing down the increase of SST. The negative SST error in the off-equatorial northern Pacific serves a complementary role in the early stages until May, reflected by the positive wind speed error index in Figure 13f, which improves the local northeasterly wind. Such variations can increase the evaporation and promote the heat released from the ocean to the atmosphere to some extent, reflected by the positive latent heat flux error index in Figure 13f. The above process propagates the negative SST error toward the central equatorial Pacific and strengthens equatorial processes, reflecting a wind–evaporation–SST (WES) (Xie & Philander, 1994) mechanism-likebehavior.

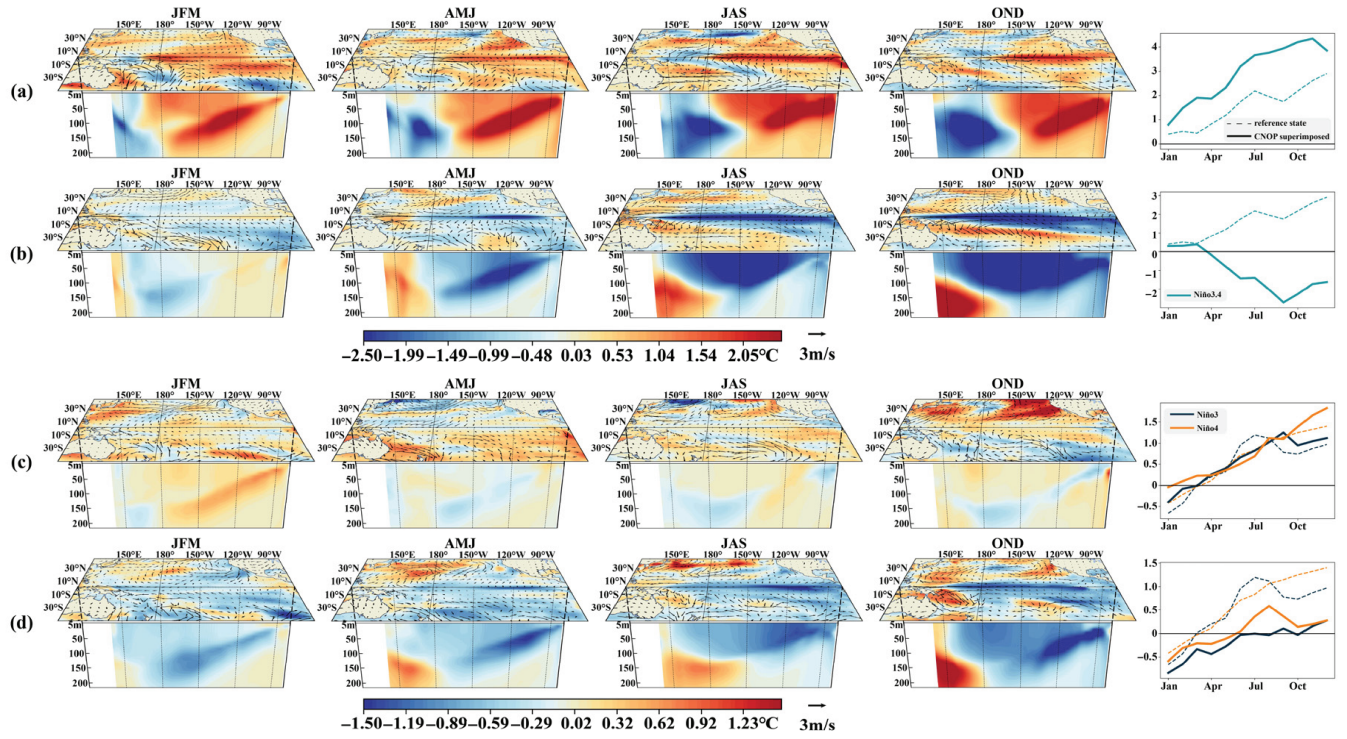

FIGURE 12 The three-month-averaged error evolutions and Niño indexes variations of corresponding optimally growing initial errors initial errors (OGIEs) in the GFDL CM2p1 model when they are superimposed into the initial conditions of two types of events. The shadings represent sea surface temperature (SST) errors and meridionally (5°N–5°N) average sea temperature errors, respectively for surface and subsurface layers in maps (a–d). The vectors represent wind errors; (a, b) are with a reference state of the eastern Pacific (EP) event, the initial condition of which is superimposed by the EP-Strengthened-OGIE and Weakened-OGIE, respectively, and (c, d) are with a reference state of the central Pacific (CP) events, the initial condition of which is superimposed by the CP-Strengthened-OGIE and Weakened-OGIE, respectively. The dotted and solid lines in the line plots represent the reference states and perturbed states, respectively. Blue/orange/green line represents the Niño3/4/3.4 index. [Colour figure can be viewed at wileyonlinelibrary.com]

As for CP-Strengthened-OGIE (Figure 12c), the amplification effects first come from the local evolution of positive SST error in the central equatorial Pacific, which induces an increase in zonal advection feedback until April (Niño4 panel in Figure 13c). During April–May–June (AMJ), the developments of positive SST error in the central Pacific become weaker, even disappear. However, from April, the positive SST error in the off-equatorial northern Pacific exhibits crucial impacts, reflected by the steadily negative wind speed error index and latent heat flux error index in Figure 13e, which induces a significant reduction on the localized trade winds, accompanied by a decrease of evaporation and less heat releasing from the ocean to the atmosphere. Such a process induces a North Pacific meridional mode (NPMM)-like pattern (Amaya, 2019; Larson & Kirtman, 2013), and propagates the warm water in the off-equatorial Pacific toward the central equatorial Pacific via the WES mechanism. When the warm SST error arrives in the central Pacific after JAS, the equatorial zonal advection feedback in the Niño4 region is improved again (Niño4 panel in Figure 13c), further promoting the SST warming over the central equatorial Pacific in the mature phase. The above processes can also explain why the variations of the Niño4 index exhibit an increase before April and after July, that is, the warming delay can be attributed to the propagation of positive SST error in the off-equatorial Pacific. Meanwhile, since extreme CP events are very rare (Figure 5e), the warming induced by this type of OGIE is limited, and cannot be compared to the EP-Strengthened-OGIE. The effects of two types of feedback are small in the Niño3 region all the time (Niño3 panel in Figure 13c).

The evolution of the dynamics of Weakened-OGIE in the CP event (Figure 12d) is almost opposite to that of CP-Strengthened-OGIE. It exhibits strong reductions of zonal advection feedback in the Niño4 region once the initial error is superimposed (Niño4 panel in Figure 13d). The negative SST error in the off-equatorial northern Pacific induces a negative NPMM-like pattern, propagating northward into the central Pacific via the WES mechanism and further promoting the cooling SST

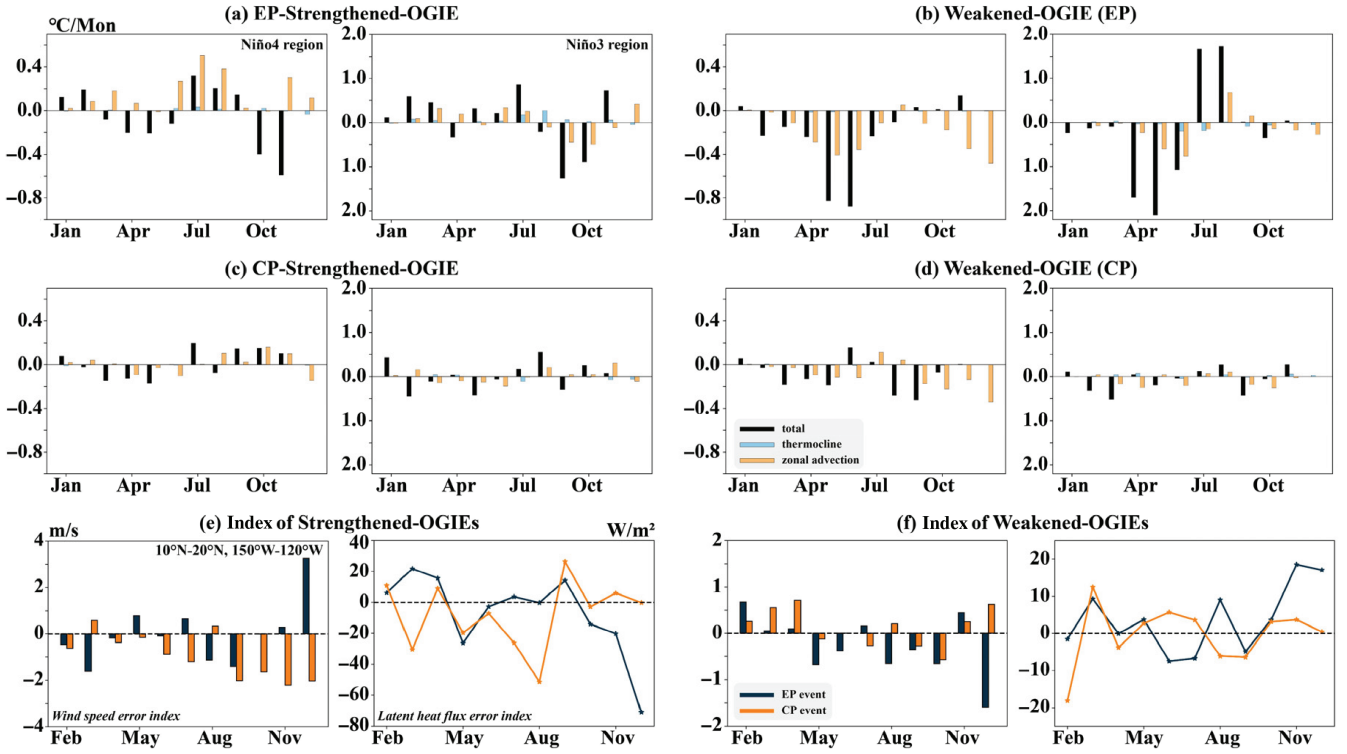

FIGURE 13 Heat budget analysis for the error evolutions of the obtained optimally growing initial errors (OGIEs) in the GFDL CM2p1 model, and the variations of two defined indices for off-equatorial processes. (a, b) The changes induced by eastern Pacific (EP)-Strengthened-OGIE and Weakened-OGIE in the EP event. (c, d) The changes induced by central Pacific (CP)-Strengthened-OGIE and Weakened-OGIE in the CP event. The black/orange/blue bars represent the variation of total temperature tendency/zonal advection feedback/thermocline feedback. Two panels in (a–d) cover the Niño4 (left) and 3 (right) regions, respectively. The two defined indices in (e,f) are wind speed error index (left bar plots) and latent heat flux error index (right line plots), respectively. They are both the average errors of the corresponding variables in the concerned region (10°N – 20°N, 150°W – 120°W). (e) With two Strengthen-OGIEs for EP (blue) and CP (orange) events, and (f) is with two Weakened-OGIEs for EP and CP events. [Colour figure can be viewed at wileyonlinelibrary.com]

(Figure 13f). In contrast to CP-Strengthened-OGIE, the negative SST errors in the central equatorial Pacific are strong enough and continue to evolve locally, with negative SST errors in the off-equatorial Pacific contributing to the process. Similarly, the effects of two types of feedback are also small in the Niño3 region (Niño3 panel in Figure 13d).

CP-Strengthened-OGIE is the newly revealed initial perturbation that influences the forecasts of CP events most. It exhibits significant errors located in two regions, the joint contribution of which can enhance the intensity of CP events in both numerical model and AI model as shown in Figure 12. To further validate the effects of off-equatorial signals, we compare the development of El Niño events due to different initial perturbations, that is, with or without the removal of the initial perturbations in the off-equatorial northern Pacific, as shown in Figure 14. The colored lines represent the development of Niño indices with initial perturbations superimposed. We find that deducting the off-equatorial signals (orange lines) can still enhance the strength of the reference state no matter in GFDL CM2p1 and ENSO-MC v2.0, but not as strongly as the original CP-Strengthened-OGIE (blue lines), suggesting the synergistic interaction of equatorial and off-equatorial signals as a key factor in error growth of CP-Strengthened-OGIE.

Our successful attempt provides a valuable insight for performing interpretability or predictability studies with an AI model, with the help of CNOP. In ENSO-MC v2.0, we infer that the tropical processes dominate OGIE evolution and the off-equatorial perturbations propagate toward the central equatorial Pacific for CP-Strengthened-OGIE and Weakened-OGIE. However, limited by the physical variables included in the AI model, we have verified the above hypothesis in a numerical model, GFDL CM2p1. As shown in Figure 12, the initial error evolutions are similar in both GFDL CM2p1 and ENSO-MC v2.0, accompanied by comprehensive analyses of heat budget and two defined off-equatorial indices (i.e., wind speed error index and latent heat flux error index).

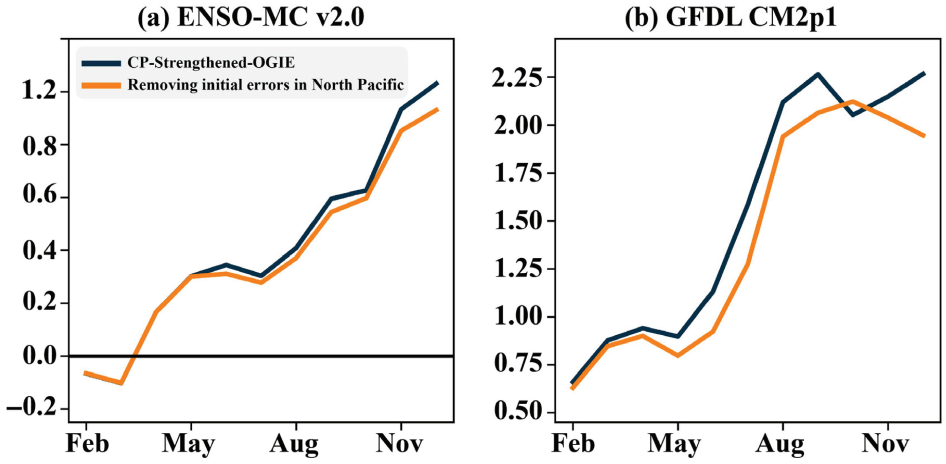

FIGURE 14 Evaluations of the Niño4 index after superimposing original central Pacific-Strengthened-optimally growing initial error (CP-Strengthened-OGIE) (blue) and removing initial errors in the off-equatorial northern Pacific (orange) into (a) El Niño-Southern Oscillation-multichannel (ENSO-MC) v2.0 and (b) GFDL CM2p1. [Colour figure can be viewed at wileyonlinelibrary.com]

In addition, we have also evaluated the simulation capability for two types of El Niño events of ENSO-MC v2.0 in Section 3.1 *Evaluations on simulation capability*, which exhibits consistent characteristics with observations. Therefore, we speculate that the evolution mechanisms of initial errors in ENSO-MC v2.0 are in line with that in GFDL CM2p1. An AI model can learn concrete mechanisms from big data to some extent. The OGIEs' spatial distributions modulate the diverse error growth mechanisms for EP and CP events. The equatorial perturbations regulate the error growths of EP-Strengthened-OGIE, and the equatorial and off-equatorial perturbations jointly contribute to the error growths of CP-Strengthened-OGIE, as well as Weakened-OGIE. These results facilitate the development of future targeted observation program.

5 | DISCUSSION AND CONCLUSION

In the big-data era, deluges of advanced deep-learning ENSO forecasting models have exhibited more skillful forecasts beyond numerical models. These models directly learn physical mechanisms hidden in data and establish a complex mapping between historical (i.e., the model's input) and future (i.e., the model's output) multivariate data. More importantly, these models usually possess higher simulation capability of El Niño diversity, significantly favoring the operational forecasts. Considering the characteristics of neural networks, the forecast errors of deep-learning models are mainly derived from the initial perturbation. Therefore, in this study, we use the superior CNOP method in a deep-learning model to perform the first kind of predictability study, revealing initial errors that affect predictions of El Niño diversity to the largest extent, which is the first successful attempt in this research field.

More specifically, we first identify several new types of OGIEs for two types of El Niño events with our proposed ENSO-MC v2.0, which represent initial perturbations that can cause the largest forecast errors under certain constraints. ENSO-MC v2.0 is a multivariate coupled model, which is the upgraded version of our previously constructed ENSO-MC. The effective forecasting lead month (i.e., the Niño3.4 index correlation skill is greater than 0.65) of this model is beyond 12, and it can reproduce two types of events that have very similar statistical properties to observations via the long-term simulations. This is also a guarantee that the predictability study can be carried out based on this model. We reveal several new types of OGIEs for two types of El Niño event in ENSO-MC v2.0 based on the CNOP method and further interpret the physical mechanisms of the OGIEs obtained in GFDL CM2p1. The results show that our obtained OGIEs keep consistent nonlinearly evolving dynamics in the numerical model, especially the ones that can strengthen CP events, which have been never investigated before. It also provides evidence of interpretability and credibility for our proposed model.

The OGIE pattern for strengthening the EP events (EP-Strengthened-OGIE) contains a significant positive SST error over the eastern equatorial Pacific, which can directly deepen the thermocline and induce the westerly wind error across the equator, further enhancing the Bjerknes feedback established in the background. The crucial distributions for the OGIE pattern that strengthens the CP events (CP-Strengthened-OGIE) are located in two positions, with one positive SST error in the central equatorial Pacific and another positive SST error in the off-equatorial northern Pacific. The former develops rapidly and locally, and the latter propagates toward the central equatorial

Pacific via the WES mechanism. These two perturbations collectively contribute to the further warming of the central equatorial Pacific. The patterns of OGIEs that weaken two types of events (Weakened-OGIE) are almost opposite to the OGIE strengthening the CP events, as well as the opposite dynamical mechanism of their evolutions. EP-Strengthened-OGIE and Weakened-OGIE are consistent with previous results obtained in other numerical models, exhibiting similar patterns and evolution mechanisms. The newly obtained CP-Strengthened-OGIE has been verified in both ENSO-MC v2.0 and GFDL CM2p1 for reliability and effectiveness by sensitivity experiments.

Our successful attempt offers an effective and dependable process of solving CNOP and performing the predictability study in a deep-learning model. On the one hand, traditional predictability studies including CNOP-based work in numerical models are usually computationally intensive (e.g., occupations of hundreds or thousands of CPU cores) and time-consuming (e.g., calculations of days or weeks) tasks, which is majorly due to the repeated integrations of numerical models both for the gradient-based and heuristic optimizations (Wang et al., 2020). In addition, gradient-based complex nonlinear problem optimization usually relies on the adjoint models, which may not be able to provide accurate gradient information for high-precision configurations (Errico, 1997) (e.g., high resolution, advanced parameterizations, etc.) in some numerical models, or even be absent (Wei et al., 2020; Yang et al., 2020, 2023). Deep-learning models intrinsically provide the interface of "automatic differentiation (Ketkar et al., 2021)," which makes the optimization of CNOP quite easier and faster. This especially favors the predictability studies for high-impact events that are difficult to simulate in numerical models, for example Madden–Julian Oscillation, Quasi-Biennial Oscillation, and so forth. It is worth noting that the used AI models should exhibit a high simulation capability beside high forecast skills for reliable predictability studies, which ensures that the development of the initial perturbation in the AI model is physically consistent with that in numerical models. The simulation capability assessments for AI models need to be further improved.

On the other hand, our study is of great significance for further improving skills of deep-learning models, beside ENSO-MC v2.0. Eliminating such initial errors in a model's input can effectively reduce forecast errors through the farsighted planning of target observation projects (Mu et al., 2015) and data assimilation, promoting "big data" to "better data." In addition, due to considerable growths of initial errors with CNOP patterns, the ensemble members derived from such spatial information have a larger spread, providing better probabilistic forecasts and more uncertainties. Note that migrating this approach to ensemble forecasts for deep-learning weather models requires some specific modifications so that the initial perturbations can exhibit significant growth (Selz & Craig, 2023). For example, decreasing the time step of deep-learning models and increasing the iteration steps can help the error to accumulate and grow.

FUNDING INFORMATION

This study is supported by the National Natural Science Foundation of China (42288101), the National Key Research and Development Program of China (2020YFA0608802), the National Natural Science Foundation of China (U2142211, 42405147, 42405048, 42475054), and the China National Postdoctoral Program for Innovative Talents (BX20230071). This study was carried out at National Supercomputer Center in Tianjin, China, supported by TianHe Qingsuo Project-special fund project in the field of climate, meteorology, and ocean.

CONFLICT OF INTEREST STATEMENT

The authors declare that they have no competing interests.

DATA AVAILABILITY STATEMENT

Data available on request from the authors.

DATA AND CODE

CMIP6 dataset: https://aims2.llnl.gov/search/cmip6; SODA dataset: https://apdrc.soest.hawaii.edu/erddap/; GODAS dataset: https://psl.noaa.gov/data/gridded/data.godas.html; ERA5 dataset: https://cds.climate.copernicus.eu/cdsapp#!/dataset/reanalysis-era5-single-levels-monthly-means?tab=form; Code: https://github.com/Skye777/ENSO-MC-v2.0.

ORCID

Bo Qin https://orcid.org/0000-0001-7093-6531

Guokun Dai https://orcid.org/0000-0001-5303-2952

REFERENCES

Amaya, D.J. (2019) The Pacific meridional mode and ENSO: a review. *Current Climate Change Reports*, 5, 296–307.

Bengio, Y., Courville, A. & Vincent, P. (2013) Representation learning: a review and new perspectives. *IEEE Transactions on Pattern Analysis and Machine Intelligence*, 35(8), 1798–1828.

Bjerknes, J. (1969) Atmospheric teleconnections from the equatorial Pacific. *Monthly Weather Review*, 97(3), 163–172.

Dai, G., Ma, X., Mu, M., Han, Z., Li, C., Jiang, Z. et al. (2023) Optimal Arctic sea ice concentration perturbation in triggering Ural blocking formation. *Atmospheric Research*, 289, 106775.

Delworth, T.L., Broccoli, A.J., Rosati, A., Stouffer, R.J., Balaji, V., Beesley, J.A. et al. (2006) GFDL's CM2 global coupled climate

models. Part I: formulation and simulation characteristics. *Journal of Climate*, 19(5), 643–674.

Duan, W. & Hu, J. (2016) The initial errors that induce a significant 'spring predictability barrier' for El Niño events and their implications for target observation: results from an earth system model. *Climate Dynamics*, 46, 3599–3615.

Duan, W., Li, X. & Tian, B. (2018) Towards optimal observational array for dealing with challenges of El Niño-southern oscillation predictions due to diversities of El Niño. *Climate Dynamics*, 51, 3351–3368.

Duan, W., Liu, X., Zhu, K. & Mu, M. (2009) Exploring the initial errors that cause a significant 'spring predictability barrier' for El Niño events. *Journal of Geophysical Research: Oceans*, 114(C4).

Duan, W., Tian, B. & Xu, H. (2014) Simulations of two types of El Niño events by an optimal forcing vector approach. *Climate Dynamics*, 43, 1677–1692.

Duan, W. & Wei, C. (2013) The 'spring predictability barrier' for ENSO predictions and its possible mechanism: results from a fully coupled model. *International Journal of Climatology*, 33(5), 1280–1292.

Duan, W. & Zhao, P. (2015) Revealing the most disturbing tendency error of Zebiak–cane model associated with El Niño predictions by nonlinear forcing singular vector approach. *Climate Dynamics*, 44, 2351–2367.

Errico, R.M. (1997) What is an adjoint model? *Bulletin of the American Meteorological Society*, 78(11), 2577–2592.

Gao, C., Chen, M., Zhou, L., Feng, L. & Zhang, R.-H. (2022) The 2020–2021 prolonged La Niña evolution in the tropical Pacific. *Science China Earth Sciences*, 65(12), 2248–2266.

Gao, C., Zhou, L. & Zhang, R.-H. (2023) A transformer-based deep-learning model for successful predictions of the 2021 second-year La Niña condition. *Geophysical Research Letters*, 50(12), e2023GL104034.

Ham, Y.-G., Kim, J.-H. & Luo, J.-J. (2019) Deep learning for multi-year ENSO forecasts. *Nature*, 573(7775), 568–572.

Ham, Y.-G. & Kug, J.-S. (2012) How well do current climate models simulate two types of El Niño? *Climate Dynamics*, 39, 383–398.

Hou, M., Duan, W. & Zhi, X. (2019) Season-dependent predictability barrier for two types of El Niño revealed by an approach to data analysis for predictability. *Climate Dynamics*, 53, 5561–5581.

Hu, J. & Duan, W. (2016) Relationship between optimal precursory disturbances and optimally growing initial errors associated with ENSO events: implications to target observations for ENSO prediction. *Journal of Geophysical Research: Oceans*, 121(5), 2901–2917.

Huang, G., Liu, Z., Van Der Maaten, L. & Weinberger, K.Q. (2017) Densely connected convolutional networks. *Proceedings of the IEEE Conference on Computer Vision and Pattern Recognition*, 4700–4708.

Iwakiri, T. & Watanabe, M. (2021) Mechanisms linking multi-year La Niña with preceding strong El Niño. *Scientific Reports*, 11(1), 17465.

Keenlyside, N.S., Latif, M. & Dürkop, A. (2007) On sub-ENSO variability. *Journal of Climate*, 20(14), 3452–3469.

Ketkar, N., Moolayil, J., Ketkar, N. & Moolayil, J. (2021) Automatic differentiation in deep-learning. In: *Deep learning with python: learn best practices of deep-learning models with PyTorch*. Berkeley, CA: Springer, pp. 133–145.

Kug, J.-S., Choi, J., An, S.-I., Jin, F.-F. & Wittenberg, A.T. (2010) Warm pool and cold tongue El Niño events as simulated by the GFDL 2.1 coupled GCM. *Journal of Climate*, 23(5), 1226–1239.

Larson, S. & Kirtman, B. (2013) The Pacific meridional mode as a trigger for ENSO in a high-resolution coupled model. *Geophysical Research Letters*, 40(12), 3189–3194.

Lee, J., Planton, Y.Y., Gleckler, P.J., Sperber, K.R., Guil'yardi, E., Wittenberg, A.T. et al. (2021) Robust evaluation of ENSO in climate models: how many ensemble members are needed? *Geophysical Research Letters*, 48(20), e2021GL095041.

Liu, Z., Mao, H., Wu, C.-Y., Feichtenhofer, C., Darrell, T. & Xie, S. (2022) A convnet for the 2020s. In: *Proceedings of the IEEE/CVF Conference on Computer Vision and Pattern Recognition*. New Orleans, LA: IEEE, pp. 11976–11986.

Lopez, H., Lee, S.-K., Kim, D., Wittenberg, A.T. & Yeh, S.-W. (2022) Projections of faster onset and slower decay of El Niño in the 21st century. *Nature Communications*, 13(1), 1915.

Lorenz, E.N. (1962) The statistical prediction of solutions of dynamical equations. In: *Proceedings of the international symposium on numerical weather prediction, 1962*. Japan: Meteor. Soc.

Mu, B., Cui, Y., Yuan, S. & Qin, B. (2022a) Simulation, precursor analysis and targeted observation sensitive area identification for two types of ENSO using ENSO-MC v1. 0. *Geoscientific Model Development*, 15(10), 4105–4127.

Mu, B., Qin, B. & Yuan, S. (2021) ENSO-ASC 1.0. 0: ENSO deep-learning forecast model with a multivariate air–sea coupler. *Geoscientific Model Development*, 14(11), 6977–6999.

Mu, B., Qin, B. & Yuan, S. (2022b) ENSO-GTC: ENSO deep-learning forecast model with a global spatial-temporal teleconnection coupler. *Journal of Advances in Modeling Earth Systems*, 14(12), e2022MS003132.

Mu, M. & Duan, W. (2003) A new approach to studying ENSO predictability: conditional nonlinear optimal perturbation. *Chinese Science Bulletin*, 48, 1045–1047.

Mu, M., Duan, W., Chen, D. & Yu, W. (2015) Target observations for improving initialization of high-impact ocean-atmospheric environmental events forecasting. *National Science Review*, 2(2), 226–236.

Mu, M., Duan, W. & Wang, B. (2003) Conditional nonlinear optimal perturbation and its applications. *Nonlinear Processes in Geophysics*, 10(6), 493–501.

Mu, M., Duan, W. & Wang, B. (2007a) Season-dependent dynamics of nonlinear optimal error growth and El Niño-southern oscillation predictability in a theoretical model. *Journal of Geophysical Research: Atmospheres*, 112(D10).

Mu, M., Xu, H. & Duan, W. (2007b) A kind of initial errors related to 'spring predictability barrier' for El Niño events in Zebiak-cane model. *Geophysical Research Letters*, 34(3).

Pegion, K., Selman, C.M., Larson, S., Furtado, J.C. & Becker, E.J. (2020) The impact of the extratropics on ENSO diversity and predictability. *Climate Dynamics*, 54, 4469–4484.

Philander, S.G.H. (1983) El Nino southern oscillation phenomena. *Nature*, 302(5906), 295–301.

Qi, Q., Duan, W. & Xu, H. (2021) The most sensitive initial error modes modulating intensities of CP-and EP-El Niño events. *Dynamics of Atmospheres and Oceans*, 96, 101257.

Ren, H.-L., Jin, F.-F., Tian, B. & Scaife, A.A. (2016) Distinct persistence barriers in two types of ENSO. *Geophysical Research Letters*, 43(20), 10–973.

Schmidhuber, J. (2015) Deep learning in neural networks: An overview. *Neural Networks*, 61, 85–117.

Selz, T. & Craig, G.C. (2023) Can artificial intelligence-based weather prediction models simulate the butterfly effect? *Geophysical Research Letters*, 50(20), e2023GL105747.

Shi, X., Chen, Z., Wang, H., Yeung, D.-Y., Wong, W.-K. & Woo, W. (2015) Convolutional LSTM network: a machine learning approach for precipitation nowcasting. In: *Advances in Neural Information Processing Systems*, Vol. 28. La Jolla, CA: NeurIPS.

Shukla, N. & Fricklas, K. (2018) *Machine learning with TensorFlow*. Shelter Island, NY: Manning Greenwich.

Stevens, E., Antiga, L. & Viehmann, T. (2020) *Deep learning with PyTorch*. Shelter Island, NY: Manning Publications.

Tao, L. & Duan, W. (2019) Using a nonlinear forcing singular vector approach to reduce model error effects in ENSO forecasting. *Weather and Forecasting*, 34(5), 1321–1342.

Tao, L., Duan, W. & Jiang, L. (2022) Model errors of an intermediate model and their effects on realistic predictions of El Niño diversity. *International Journal of Climatology*, 42(15), 7443–7464.

Tao, L., Duan, W. & Vannitsem, S. (2020) Improving forecasts of El Niño diversity: a nonlinear forcing singular vector approach. *Climate Dynamics*, 55, 739–754.

Tao, L., Mu, M., Wang, L., Fang, X., Duan, W. & Zhang, R.-H. (2023) Impacts of initial zonal current errors on the predictions of two types of El Niño events. *Journal of Geophysical Research: Oceans*, 128(6), e2023JC019833.

Vimont, D.J., Alexander, M.A. & Newman, M. (2014) Optimal growth of central and east Pacific ENSO events. *Geophysical Research Letters*, 41(11), 4027–4034.

Wang, Q., Mu, M. & Dijkstra, H.A. (2013) The similarity between optimal precursor and optimally growing initial error in prediction of Kuroshio large meander and its application to targeted observation. *Journal of Geophysical Research: Oceans*, 118(2), 869–884.

Wang, Q., Mu, M. & Sun, G. (2020) A useful approach to sensitivity and predictability studies in geophysical fluid dynamics: conditional non-linear optimal perturbation. *National Science Review*, 7(1), 214–223.

Wei, Y., Mu, M., Ren, H.-L. & Fu, J.-X. (2019) Conditional nonlinear optimal perturbations of moisture triggering primary MJO initiation. *Geophysical Research Letters*, 46(6), 3492–3501.

Wei, Y., Ren, H.-L., Mu, M. & Fu, J.-X. (2020) Nonlinear optimal moisture perturbations as excitation of primary MJO events in a hybrid coupled climate model. *Climate Dynamics*, 54, 675–699.

Xie, S.-P. & Philander, S.G.H. (1994) A coupled ocean-atmosphere model of relevance to the ITCZ in the eastern Pacific. *Tellus A*, 46(4), 340–350.

Xu, H., Chen, L. & Duan, W. (2021) Optimally growing initial errors of El Niño events in the CESM. *Climate Dynamics*, 56(11–12), 3797–3815.

Yang, Z., Fang, X. & Mu, M. (2020) The optimal precursor of El Niño in the GFDL CM2p1 model. *Journal of Geophysical Research: Oceans*, 125(3), e2019JC015797.

Yang, Z., Fang, X. & Mu, M. (2023) Optimal precursors for central Pacific El Niño events in GFDL CM2p1. *Journal of Climate*, 36(10), 3453–3467.

Yu, J.-Y., Wang, X., Yang, S., Paek, H. & Chen, M. (2017) The changing El Niño–southern oscillation and associated climate extremes. In: *Climate Extremes: Patterns and Mechanisms*. Hoboken, NJ: Wiley Online Library, pp. 1–38.

Zhang, C., Bengio, S., Hardt, M., Recht, B. & Vinyals, O. (2021) Understanding deep-learning (still) requires rethinking generalization. *Communications of the ACM*, 64(3), 107–115.

Zhang, R.-H., Zhou, L., Gao, C. & Tao, L. (2024) A transformer-based coupled ocean-atmosphere model for ENSO studies. *Science Bulletin*, S2095–S9273. https://doi.org/10.1016/j.scib.2024.04.048

Zhou, L. & Zhang, R.-H. (2023) A self-attention–based neural network for three-dimensional multivariate modeling and its skillful ENSO predictions. *Science Advances*, 9(10), eadf2827.

How to cite this article: Qin, B., Yang, Z., Mu, M., Wei, Y., Cui, Y., Fang, X. *et al.* (2024) The first kind of predictability problem of El Niño predictions in a multivariate coupled data-driven model. *Quarterly Journal of the Royal Meteorological Society*, 1–20. Available from: https://doi.org/10.1002/qj.4882

APPENDIX A

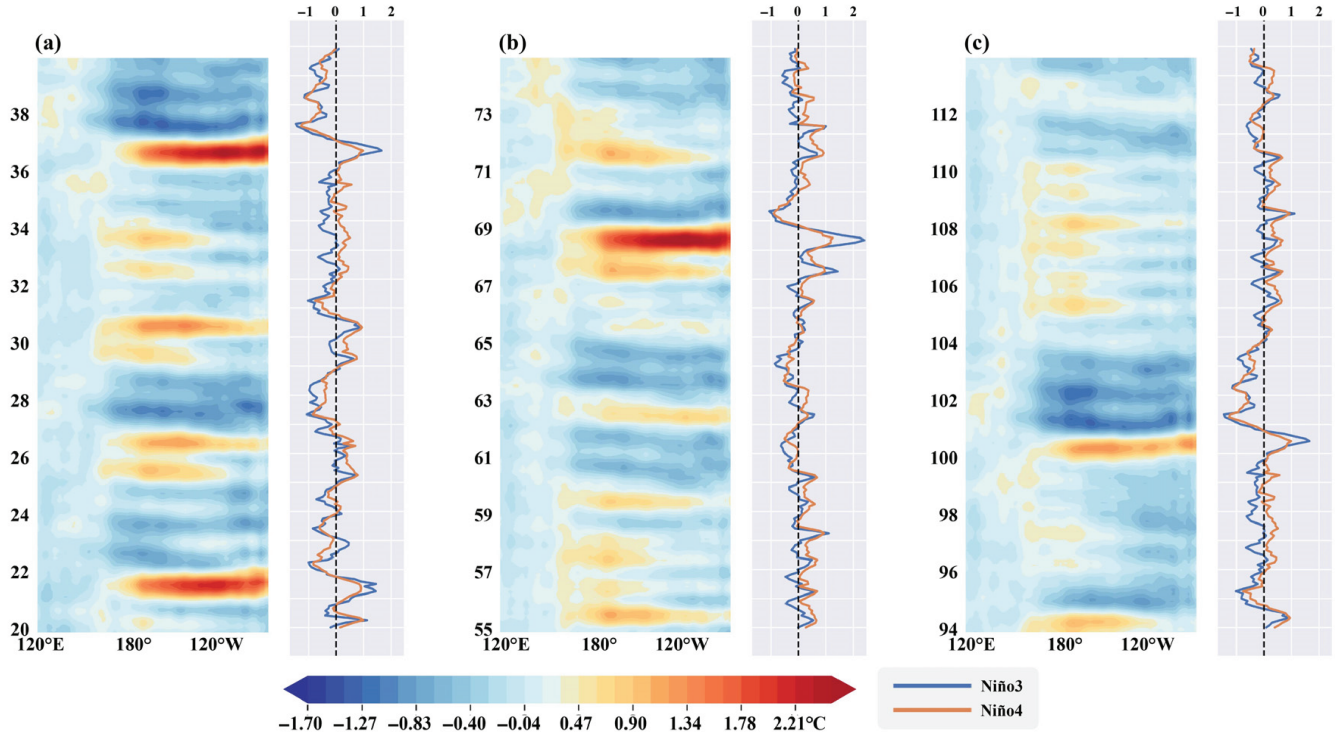

FIGURE A1 Three 20-year simulating segments taken from the 12,000-year long-term simulations. The left and right columns in every segment are respectively the Hovmöller diagrams and the corresponding variations of the Niño3 (blue) and 4 (red) indexes. [Colour figure can be viewed at wileyonlinelibrary.com]

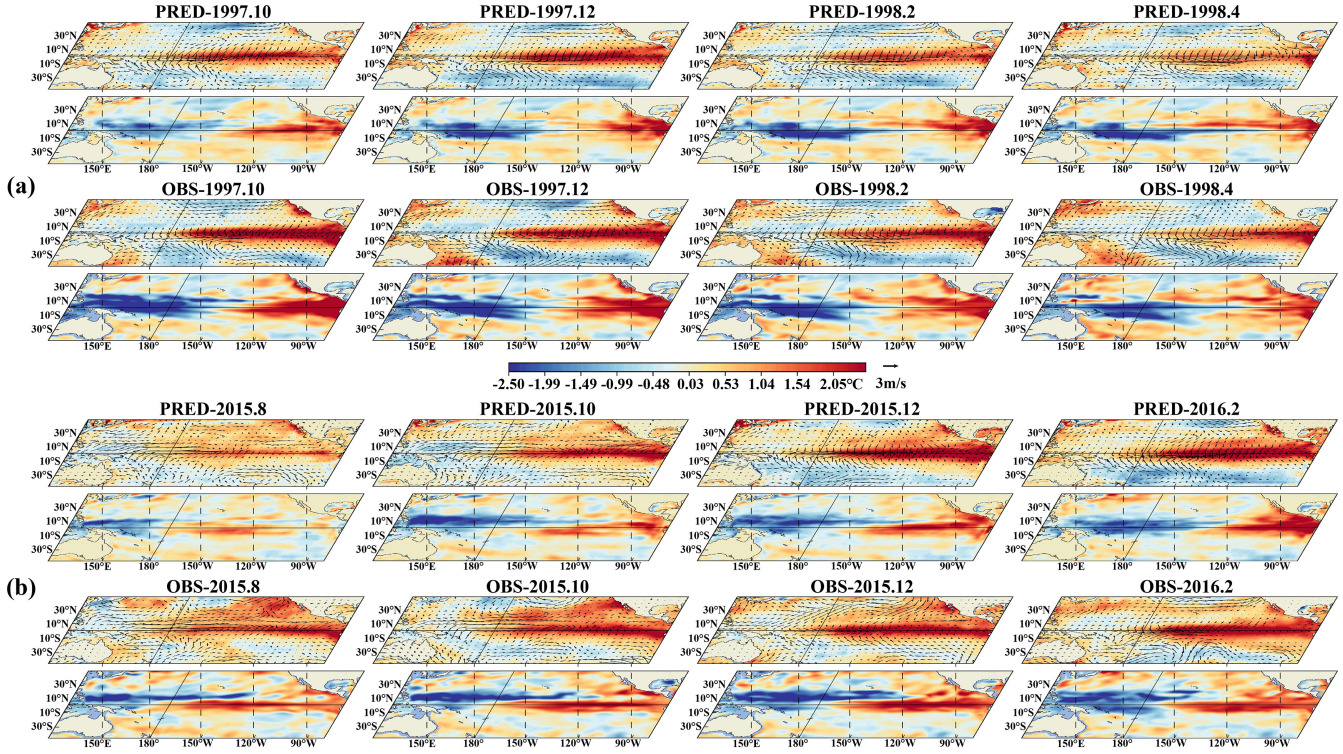

FIGURE A2 Two simulating monthly results for (a) 97/98 and (b) 15/16 EP events. Both simulations are obtained at a 12-month leading (i.e., starting forecasting from 1997.4 and 2016.2). The above and down rows in each simulation are respectively the prediction result and observations. [Colour figure can be viewed at wileyonlinelibrary.com]

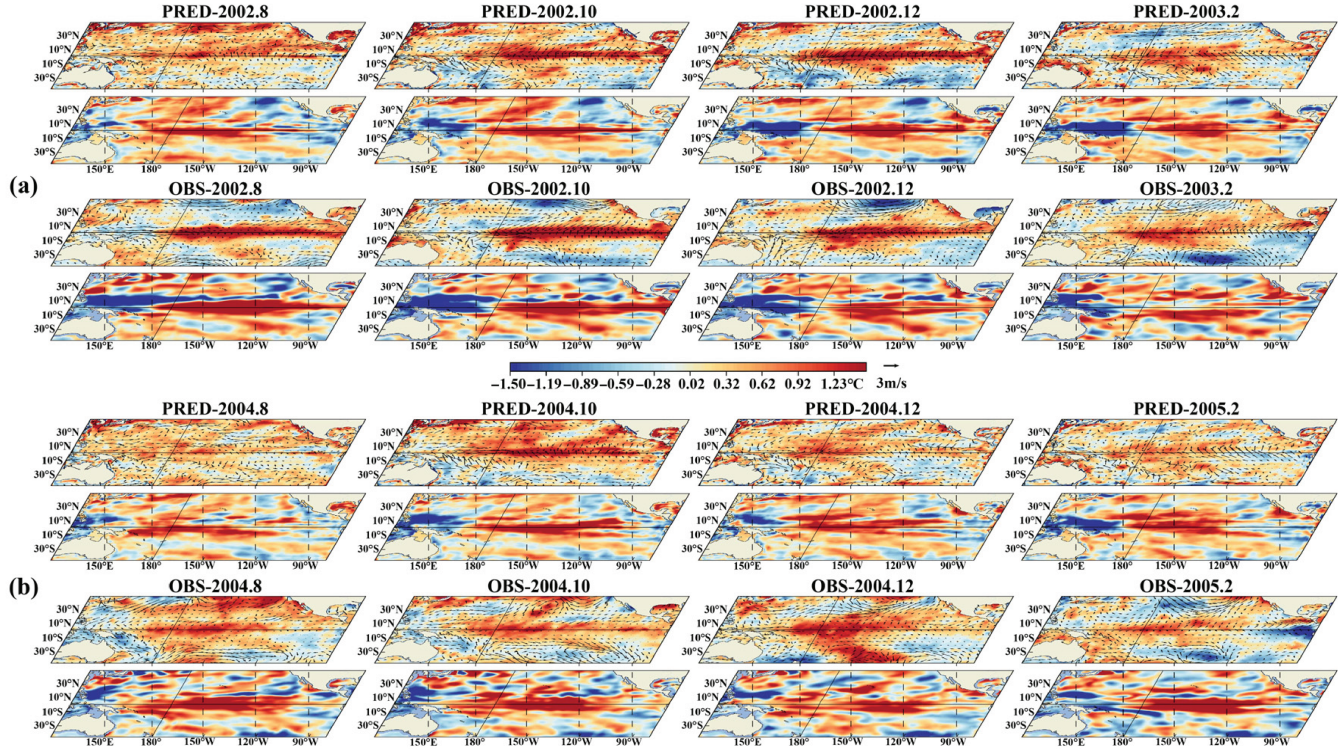

FIGURE A3 Two simulating monthly results for (a) 02/03 and (b) 04/05 CP events. Both simulations are obtained at a 12-month leading (i.e., starting forecasting from 2002.2 and 2004.2). The above and down rows in each simulation are respectively the prediction result and observations. [Colour figure can be viewed at wileyonlinelibrary.com]